Axial Synchronous Current Suppression of Maglev High-speed Motor Using Adaptive Notch Filter

Yue Zhang[1], Jin Zhou[1], Xudong Guan[1], Yuanping Xu[1], Chaowu Jin[1] and Yingzhe Lin[2]

[1] Nanjing University of Aeronautics and Astronautics, Nanjing, China
[2] Nanjing CIGU Technology Corp., Ltd., Nanjing, China
zhangyue08@nuaa.edu.cn

Abstract

Affected by the radial coupling disturbance, the axial displacement of the active magnetic bearings (AMBs) system will contain the rotation speed signal, which may lead the power amplifier saturation when the maglev high-speed motor rotates at high speed. To solve this issue, an axial synchronous current suppression method based on adaptive notch filter (ANF) combined with speed estimation algorithm is proposed in this paper and the influence of ANF parameters on the estimation result is analyzed. Simulation and experimental results show that the proposed method can estimate the rotational speed accurately and suppress the axial synchronous current effectively, ensuring the high speed and stable operation of the maglev high-speed motor.

1 Introduction

AMBs have been increasingly applied in high-speed motors and drawn attention in the field of turbine machinery because of its non-contact and non-lubricating [1]. The maglev high-speed motor is connected to the load in a direct drive manner. Affected by airflow disturbances, the vibration amplitude of the rotor near the impeller is larger than that of the rotor away from the impeller, which will cause the coupling of radial and axial AMBs. As a result, the rotor axial displacement signal contains a sinusoidal signal with the same frequency as the speed. Due to the difference in structure and design, the differential coefficient of the axial AMB system is generally several times that of the radial AMB system when the decentralized PID control is used. The differential link has an amplification effect on the high frequency signal. The amplitude of the axial control current will be very large at high speed, which makes the axial power amplifier saturated earlier than radial power amplifier. That is not conducive to the high speed and stable operation of the maglev high-speed

motor. The suppression of axial synchronous current plays an important role in the high speed rotation of the maglev high-speed motor.

The notch filter is widely used in the unbalance control of AMBs and its function is to extract and filter out the synchronous signal. However, it requires the rotating speed sensor to provide the rotational frequency. Rotating speed sensors are not available generally in the maglev high-speed motors due to the structure limitation and high operating temperature. In addition, the sensorless vector control (SLVC) method is generally used in high-speed motors. Frequency estimation and signal extraction for sinusoidal signals with unknown parameters are feasible, such as phase-locked loop [3], frequency-locked loop [4], Kalman filter [5], LMS algorithm [6], short-time Fourier transform [7] and so on. In the application of magnetic bearings, reference [8] proposed two adaptive observers to estimate the unbalanced signal frequency and amplitude of the magnetic levitation system, but did not consider the influence of signal harmonics and noise on the estimation process. Reference [9] proposed an adaptive frequency estimator that uses the displacement signals of one radial AMB in two directions to estimate the speed. Reference [10] proposed an improved method on the basis of [9] that added phase shift compensation to keep the system stable in a large operating speed range. However, the adaptive frequency estimator requires the amplitudes of the displacement signals in the two directions to be the same, which is difficult to achieve in the AMB system. In response to this problem, reference [11] proposed an improved Hilbert transform method, which only uses one direction displacement signal for estimation. This method has high accuracy, but the algorithm is complex and the calculation amount is large.

In addition, reference [12] proposed an improved adaptive estimation method to estimate the surge frequency and amplitude of the maglev blower, eliminating the influence of signal amplitude on the estimated speed. However, this method is only used for open-loop detection, and is not used for closed-loop control. The above references all use the radial displacement signal for frequency estimation and unbalance compensation, and do not consider the influence of the axial Synchronous current.

This paper proposes a method of speed estimation and axial synchronous current suppression based on discrete ANF for maglev high-speed motor without a rotational speed sensor. The axial displacement signal is used to estimate the rotor speed, and the axial synchronous control current is filtered out to avoid the saturation of the power amplifier. The experimental results measured on the designed maglev high-speed motor prove the effectiveness of this method.

2 Speed Estimation and Synchronous Current Suppression

Affected by the radial coupling disturbance, the rotor axial displacement of the AMB system will produce sinusoidal fluctuations. Let the rotor axial displacement signal be

$$x(k) = A\sin(\omega_0 k + \theta) + v_0(k),\ \ k = 1,2,\dots,N \tag{1}$$

where ω_0 is the speed frequency, A and θ is the amplitude and initial phase of the synchronous displacement signal respectively, $v_0(k)$ is an additive gaussian white noise.

The transfer function of the second-order IIR ANF is

$$H(z,a) = \frac{N(z,a)}{D(z,a)} = \frac{1+az^{-1}+z^{-2}}{1+\rho az^{-1}+\rho^2 z^{-2}} \tag{2}$$

where ρ controls the notch bandwidth of the ANF, $0 < \rho < 1$. The larger the ρ, the smaller the notch bandwidth is. $a = -2\cos\tilde{\omega}$ is the adaptive adjustment parameter of the ANF. In the adaptive adjustment process, a keeps approaching $a_0 = -2\cos\omega_0$, making the center frequency of the ANF equal to the frequency of the input signal. Define $w(k)$ as the internal state of the ANF, and $y(k)$ as the output of the ANF, then

$$w(k) = \frac{1}{D(z,a)}x(k) = x(k) - \rho a w(k-1) - \rho^2 w(k-2) \tag{3}$$

$$y(k) = H(z,a)x(k) = w(k) + aw(k-1) + w(k-2) \tag{4}$$

The estimated recursive formula for the adaptive adjustment parameter a is [13]

$$a(k+1) = a(k) - \mu D(k) \tag{5}$$

$$D(k) = \arctan\left[\frac{y(k)}{x(k)+c}\right] \tag{6}$$

where μ is a positive number that controls the convergence speed, and c is a small constant to prevent a singularity of the ratio. In the steady state, $|y(k)|$ is always smaller than $|x(k)|$, then $-1 \leq y(k)/x(k) \leq 1$. At this time, Eq. (6) can be approximately expressed as

$$D(k) \approx \frac{\frac{y(k)}{x(k)}}{1+\alpha\left(\frac{y(k)}{x(k)}\right)^2} = \frac{x(k)y(k)}{x^2(k)+\alpha y^2(k)} \tag{7}$$

where $\alpha = 9/32$. Then Eq. (5) can be approximately expressed as

$$a(k+1) = a(k) - \mu \frac{x(k)y(k)}{x^2(k)+\alpha y^2(k)} \tag{8}$$

The rotational speed frequency can be obtained by

$$f = \frac{f_s}{2\pi}\arccos\left(-\frac{a}{2}\right) \tag{9}$$

where f_s is the sampling frequency.

From the transfer function of the ANF, the amplitude-frequency response and phase can be obtained as

$$|H(z,a)| = \frac{|2\cos\omega_0 + a|}{\sqrt{[(\rho^2+1)\cos\omega_0 + \rho a]^2 + [(1-\rho^2)\sin\omega_0]^2}} \tag{10}$$

$$\phi = \begin{cases} -\arctan\frac{(1-\rho^2)\sin\omega_0}{(\rho^2+1)\cos\omega_0+\rho a} & \omega_0 \leq \frac{\pi}{2} \\ \pi + \arctan\frac{(1-\rho^2)\sin\omega_0}{(\rho^2+1)\cos\omega_0+\rho a} & \omega_0 > \frac{\pi}{2} \end{cases} \tag{11}$$

The real frequency characteristic is

$$\mathrm{Re}\{H(z,a)\} = \frac{(2\cos\omega_0+a)[(\rho^2+1)\cos\omega_0+\rho a]}{[(\rho^2+1)\cos\omega_0+\rho a]^2+[(1-\rho^2)\sin\omega_0]^2} \tag{12}$$

Let

$$D(k) = \arctan\left[\frac{y(k)}{x(k)}\right] = \arctan(\mathrm{Re}\{H(z,a)\}) = 0 \tag{13}$$

Then

$$(2\cos\omega_0 + a)[(\rho^2+1)\cos\omega_0 + \rho a] = 0 \tag{14}$$

It is easy to prove that $(\rho^2+1)\cos\omega_0 + \rho a \neq 0$. If and only if $a = -2\cos\omega_0$, Eq. (14) holds, that is, $\tilde{\omega} = \omega_0$. When $\tilde{\omega} > \omega_0$, $D(k) > 0$, a tends to decrease, and $\tilde{\omega}$ decreases; when $\tilde{\omega} < \omega_0$, $D(k) < 0$, a tends to increase, and $\tilde{\omega}$ increases. After constant adjustment, $\tilde{\omega}$ will eventually stabilize at the optimal solution ω_0, that is, the estimated frequency converges to the speed frequency.

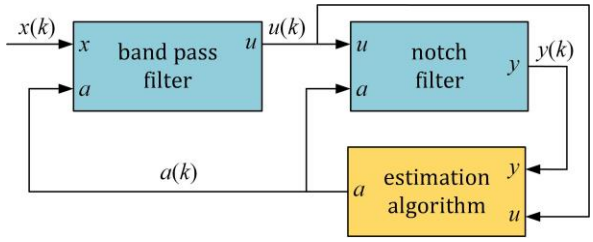

Fig.1 Structure of adaptive notch filter

There are harmonics and noise signals superimposed on the displacement signal. This will cause a certain deviation and a small oscillation of the estimated frequency. In order to reduce the interference of harmonics and noise, a band-pass filter can be added to the signal input for pre-filtering. As shown in Fig.1, the center frequencies of the band-pass filter and the notch filter are the same, which change

with the iteration of the estimation algorithm. The output $u(k)$ of the bandpass filter is the synchronous component in the input signal at steady state, which can be expressed as:

$$u(k) = [1 - H(z, a)]x(k) \tag{15}$$

Fig.2 is the diagram of axial AMB control system with ANF. The difference between the axial sensor output and the reference position is used as the input of the ANF. After calculation, the rotation speed and the extracted synchronous component are output, and the synchronous component is subtracted from the controller input signal. Then after the controller and the power amplifier, the output control current does not include the current with the same frequency as the speed, and the synchronous current suppression is realized.

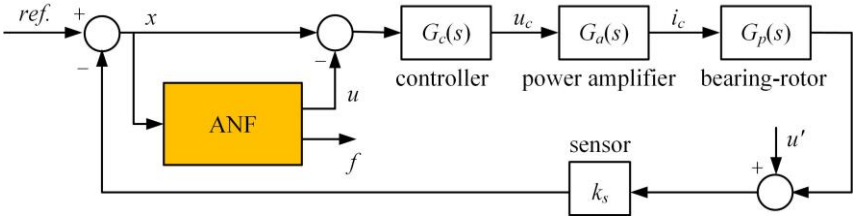

Fig.2 Diagram of axial AMB system with ANF

3 Simulation results

The axial displacement signal of the magnetic levitation rotor not only contains the sinusoidal signal with the same frequency as the speed, but also contains harmonics and noise signals. Since the harmonic signal has a small amplitude compared with the fundamental frequency signal, the input signal of the ANF used in the simulation is

$$x = \sin(2\pi ft) + 0.3\sin(6\pi ft) + 0.1\sin(10\pi ft) + v \tag{16}$$

Take $\rho = 0.97$, $\mu = 0.001$. The speed frequency f is initially 300Hz, after 1s it becomes 400Hz, and after 3s it becomes 500Hz. The frequency estimation is carried out using the proposed method, as shown in Figure 3. It can be seen that the estimated frequency can converge to the speed frequency within 0.4s. Figure 4 is a section of input and output signals when the rotation speed is 400Hz. After the input signal passes through the ANF, the fundamental frequency signal of the rotation speed can be extracted.

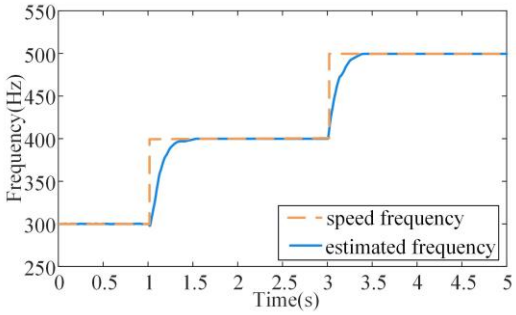

Fig.3 Simulation result of frequency estimation

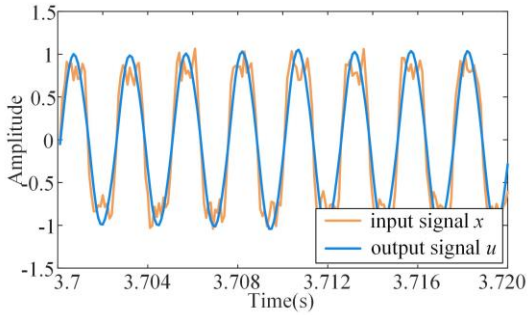

Fig.4 Input and output signal comparison

There are two adjustable parameters ρ and μ in the ANF, which will affect the estimation results. When $\mu = 0.001$ and the rotational speed frequency is 300 Hz, the estimation results of different ρ are shown in Fig.5. When ρ is too small, errors will occur in the estimation results. When ρ is too large, the closer to 1, the higher the estimation accuracy is. However, at this time, the notch width is too narrow, and the robustness of the algorithm will be reduced, or even no convergence. Therefore, the value of ρ is generally 0.92~0.98.

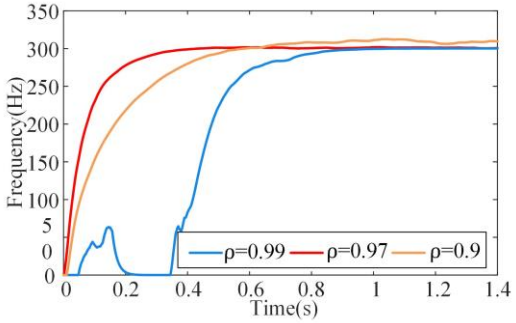

Fig.5 The influence of different ρ on the estimation results

When $\rho = 0.97$ and the rotating speed frequency is 300Hz, the estimation results of different μ are shown in Fig.6. When μ is too large, the response speed is faster, but the result will be oscillation and have poor anti-interference ability. When μ is too small, the steady-state performance is better and the accuracy is higher, but the response speed is slower. Therefore, it is necessary to choose the appropriate μ to meet the requirements of accuracy and speed.

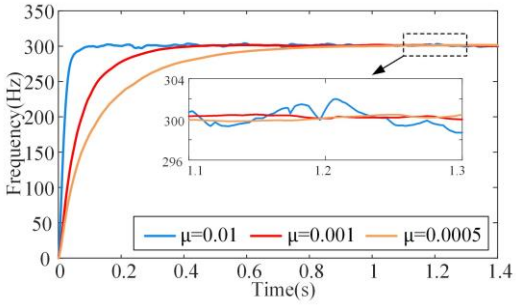

Fig.6 The influence of different μ on the estimation results

4 Experimental results

In order to verify the effectiveness of the proposed method, a maglev high-speed motor is used for experiments. The experimental rig is shown in Fig.7. The controller uses dSPACE 1202 with a sampling frequency of 20kHz, which outputs a control voltage signal. The power amplifier outputs control current signals to control the AMB coils so that the rotor is suspended at a set position. Decentralized PID control is adopted for the radial and axial AMBs to realize the rotor stable suspension.

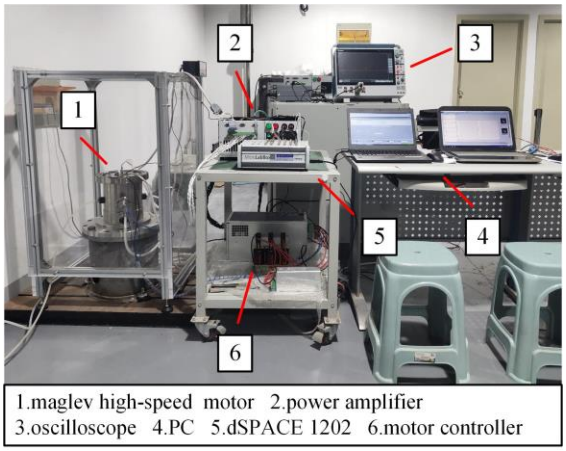

Fig.7 Maglev high-speed motor test rig

The parameters of the axial AMB system are shown in Table 1. The transfer functions of the axial controller, power amplifier, and bearing-rotor are respectively

$$G_c(s) = k_P + \frac{k_I}{s} + \frac{k_D s}{T_D s+1} \tag{17}$$

$$G_a(s) = \frac{k_a}{T_a s+1} \tag{18}$$

$$G_p(s) = \frac{k_i}{ms^2+k_x} \tag{19}$$

Table 1 The parameters of the axial AMB system

Parameters	Value	Unit
m	3.58	Kg
k_i	264.12	N/A
k_x	-0.73	N/μm
k_P	1.4	/
k_I	1	/
k_D	0.005	/
T_D	0.0001	/
k_a	0.4	A/V
T_a	0.0001	/
k_s	3450	V/m
i_0	2	A

The motor rotor and AMBs configuration used in the experiment are shown in Fig.8. Due to the limitation of the motor internal space, the speed sensor cannot be installed. The axial displacement sensor is installed at the end of the impeller, and the measured axial displacement is greatly affected by the radial direction.

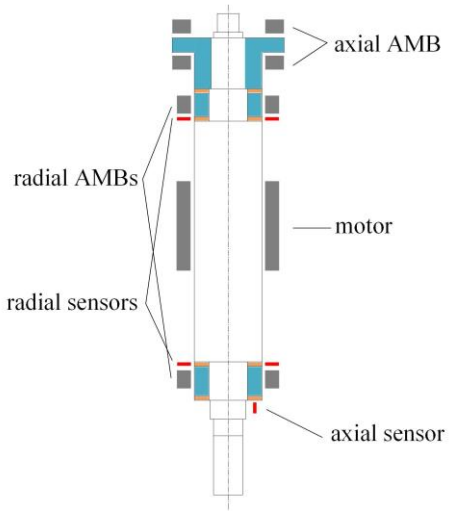

Fig.8 Structure diagram of maglev high-speed motor

Fig.9 and Fig.10 are the time-domain and frequency-domain diagrams of the axial displacement and radial displacement when the ANF is not used. It can be seen that the main components of the axial and radial displacement signals are sinusoidal signals with a frequency of 500 Hz. As we all know, the main component in the radial displacement signal is the unbalanced vibration caused by the rotor unbalanced mass, and its frequency is the same as the speed frequency. Therefore, the main component in the axial displacement signal is also the same as the speed frequency. It can be seen from the time domain diagram that, compared with the radial displacement signal, the axial displacement signal has less harmonics and noise. Using the axial displacement signal to estimate the rotor speed will be more accurate.

Firstly, the feasibility of the proposed method is investigated at a fix speed. Because the bias current of the axial AMB is 2A, theoretically the maximum amplitude of the coil control current is 2A, otherwise it will cause the saturation of the power amplifier. In fact, because of the electromagnetic noise, sensor measurement error and other reasons, the maximum allowable control current amplitude will be smaller. The maglev high-speed motor used in the experiments is a vertical structure. In order to counteract gravity, there will still have an offset of about 0.35A in the axial control current, which leads to further restrictions on the maximum allowable control current.

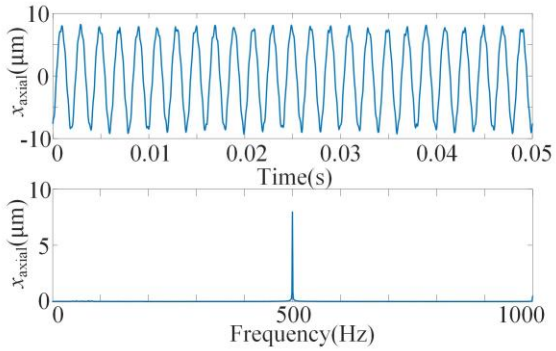

Fig.9 Time and frequency domain diagrams of the axial displacement

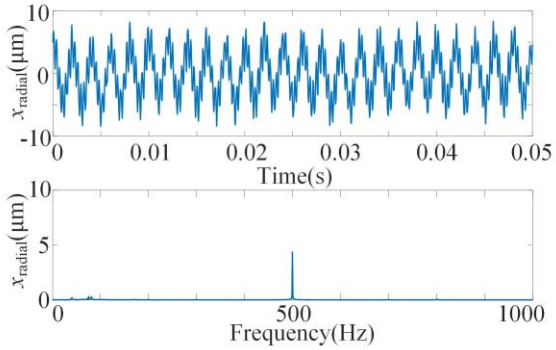

Fig.10 Time and frequency domain diagrams of the radial displacement

Fig.11 is a comparison diagram of the time domain and frequency domain of the axial AMB control current without and with ANF. It can be seen from the frequency domain diagram that the rotor speed at this time is 30000rpm (500Hz). Fig.12 shows the speed frequency estimated by the ANF. It fluctuates around 500Hz with a fluctuation range of ±0.1Hz, which proves the accuracy of the proposed method. When the ANF is not used at 30000rpm, the axial AMB control current is close to 2A. There is a risk of instability if the speed continues to increase. After using the ANF, the amplitude of the synchronous control current is reduced by 78%, from 1A to 0.22A.

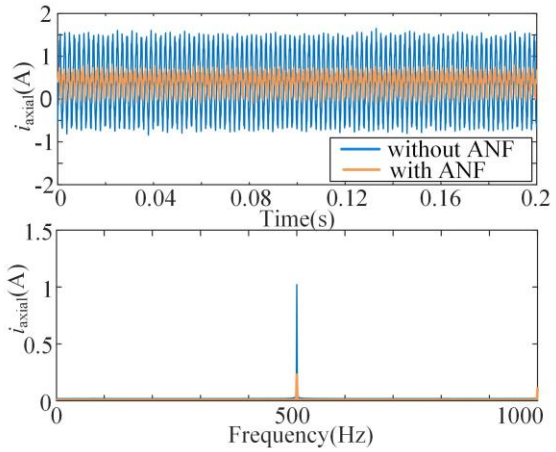

Fig.11 The coil current without and with ANF

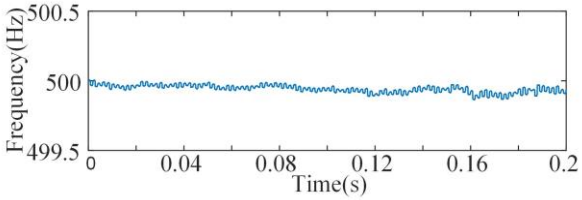

Fig.12 Experimental result of speed estimation

To make the rotor run at high speed, it is necessary to use the ANF during the speed-up process. Since the notch filter may cause the rotor unstable below the rigid body modal frequency, it is set to suppress the axial current when the estimated speed is above 20,000 rpm. Fig.13 shows the synchronous control current of the axial AMB without ANF. It can be seen that the amplitude of the axial synchronous current becomes larger and larger as the rotational speed increases, reaching 1.1A at 35,000 rpm.

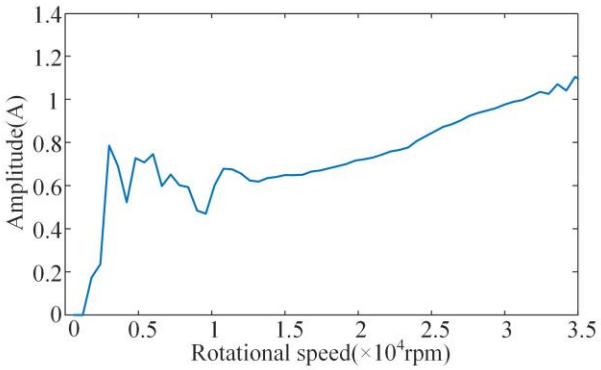

Fig.13 Axial synchronous current amplitude without ANF

As shown in Fig.14, the amplitude of the axial synchronous current still increases with the increase of the rotational speed after 20,000rpm. However, it is much smaller than when the ANF is not used. Experiments have shown that the use of ANF for axial synchronous current suppression avoids the premature saturation of the axial power amplifier. As a result, the maglev high-speed motor can run stably at 80,000rpm and the maximum speed reaches 85,000 rpm.

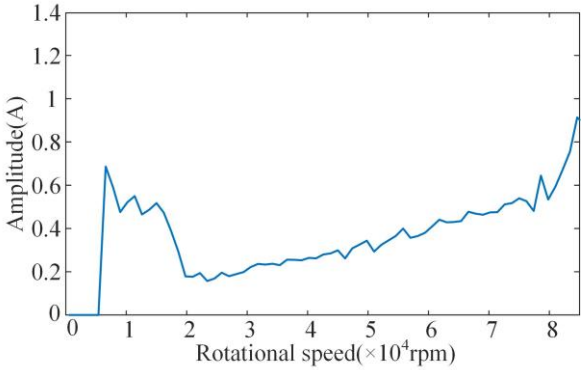

Fig.14 Axial synchronous current amplitude with ANF

5 Conclusion

This paper presents a method of speed estimation and axial synchronous current suppression for maglev high-speed motors using adaptive notch filter. This method uses the rotor axial displacement signal to estimate the rotor speed without a rotating speed sensor. In addition, the axial AMB synchronous current is suppressed to avoid the power amplifier saturation and ensure the high speed and stable operation of the maglev high-speed motor with a maximum speed of 85,000 rpm.

References

[1] Schweitzer G, Maslen E, Bleuler H, et al (2009). *Magnetic Bearing: Theory, Design, and Application to Rotating Machinery*. Berlin, Germany: Springer.

[2] Herzog R, Buhler P, Gahler C, et al (1996). *Unbalance compensation using generalized notch filters in the multivariable feedback of magnetic bearings*. IEEE Transactions on Control

Systems Technology, 4(5), pp. 580-586.
[3] Karimi-Ghartemani M, Karimi H, Iravani M R (2004). *A magnitude/phase-locked loop system based on estimation of frequency and in-phase/ quadrature-phase amplitudes*. IEEE Transactions on Industrial Electronics, 51(2), pp. 511-517.
[4] Rodriguez P, Luna A, Candela I, et al (2011). *Multiresonant Frequency-Locked Loop for Grid Synchronization of Power Converters Under Distorted Grid Conditions*. IEEE Transactions on Industrial Electronics, 58(1), pp. 127-138.
[5] Dhaouadi R, Mohan N, Norum L (1991). *Design and implementation of an extended Kalman filter for the state estimation of a permanent magnet synchronous motor*. IEEE Transactions on Power Electronics, 6(3), pp. 491-497.
[6] Wang J, Shen W, Zhao J (2007). *Adaptive adjustment of maneuvering frequency in target tracking*[J]. Transaction of Beijing Institute of Technology, 1, pp. 42-45.
[7] Borkowski J, Kania D, Mroczka J (2014). *Interpolated DFT-Based Fast and Accurate Frequency Estimation for the Control of Power*. IEEE Transactions on In-dustrial Electronics, 61(12), pp. 7026-7034.
[8] Vahedforough E, Shafai B, Beale S (2007). *Estimation and rejection of unknown sinusoidal disturbances using a generalized adaptive forced balancing Method*. IEEE American Control Conference.
[9] Chen Q, Liu G, Han B (2015). *Suppression of Imbalance Vibration in AMB-Rotor Systems Using Adaptive Frequency Estimator*. IEEE Transactions on Industrial Electronics, 62(12), pp. 7696-7705.
[10] Chen Q, Liu G, Han B (2017). *Unbalance vibration suppression for AMBs system using adaptive notch filter*. Mechanical Systems and Signal Processing, 93, pp. 136-150.
[11] Zhang R, Liu H, Fan Y (2017). *Estimation method of rotor speed using signal of displacement sensor in magnetic suspension flywheel*. Journal of Astronautics, 38(12), pp. 1314-1323.
[12] Han B, Wang K, Zheng S, Zhang Y (2017). *Surge detection of magnetically suspended high-speed centrifugal blower*. Optics and Precision Engineering, 4.
[13] Punchalard R (2014). *A modified inverse tangent based adaptive algorithm for a second-order constrained adaptive IIR notch filter*. Signal Processing, 94, pp. 350-358.